Journal of Applied Fluid Mechanics, Vol. 11, No. 6, pp. 1489-1495, 2018.
Available online at www.jafmonline.net, ISSN 1735-3572, EISSN 1735-3645.
DOI: 10.29252/jafm.11.06.29115

Reduction of Aerodynamic Drag Force for Reducing Fuel Consumption in Road Vehicle using Basebleed

G. Sivaraj[1†], K. M. Parammasivam[2] and G. Suganya[1]

[1] *Department of Aeronautical Engineering, Bannari Amman Institute of Technology, Sathyamangalam, Tamilnadu, 638401, India*
[2] *Department of Aerospace Engineering, Anna University MIT Campus, Chennai, Tamilnadu, 600044, India*

†*Corresponding Author Email: sivarajg@bitsathy.ac.in*

ABSTRACT

This paper presents the study of the overall aerodynamic performance of road vehicles and suggests a method to reduce the drag force and also to find the optimum location for placing basebleed in a car using aerodynamic principle. The overall aerodynamic drag force is reduced by eliminating wake region at the rear side of the car and reducing pressure in the front region of the car by delaying the flow separation. This improves the overall aerodynamic performance of the car thereby reducing fuel consumption, as well as improving stability and comfort by the attachment of basebleed. The wind tunnel tests are conducted for a subscale model of car with the basebleed at various locations along the front and rear side of the car in both X and Y directions. The coefficient of drag (C_D), the coefficient of lift (C_L) and coefficient of side force (C_S) for the car is measured to interpret the effect of flow conditions on the car model. The experimental result reveals that the attachment of base bleed at an optimum position in the front and rear side of the car improves its performance and decreases drag coefficient by 6.188 %.

Keywords: Road vehicle; Wind tunnel; Basebleed; Aerodynamic drag force; Pressure coefficient; Fuel consumption.

NOMENCLATURE

A_f	frontal area of the car	FC	fuel consumption
B_f	distance between basebleed tubes at the front side	H_f	distance between road surface to the base bleed at the front side
B_r	distance between basebleed tubes at the rear side	H_r	distance between road surface to the base bleed at the rear side
C_D	coefficient of drag	L	lift force
C_L	coefficient of lift	S	side force
C_p	coefficient of pressure	U	air velocity (Car speed in real condition)
C_S	coefficient of side force	ρ	density of air
D	drag force	η	the property of dthe riving vehicle

1. INTRODUCTION

In the contemporary world, safety, performance, and comfort of road vehicles are essential parameters. At the same time, low fuel consumption is of crucial importance for developing countries like India because it supports the economy of the country. In India, most of the vehicles are petroleum based and the average fuel consumption of petroleum is 4.1 million barrel per day and every year fuel consumption is increasing alarmingly at 5%. Hence researchers are working to reduce the fuel consumption of the road vehicle, even a small amount of reduction will be a great achievement. Nowadays automobile industries are concentrating on designing the vehicle with better fuel consumption to attract the market. Conventional ways to reduce the fuel consumption of the vehicle was to reduce its overall weight, modifying the engine volume (cc), engine combustion process, etc., which will directly affect its comfort and performance. In the current work, importance was given to reduce the fuel consumption of road vehicle (hatchback car) without disturbing its performance and comfort to the passenger. Aerodynamic studies on hatchback car were conducted for improving both parameters simultaneously. Hatchback car was chosen because which is preferred by most of the economic loving people.

Aerodynamics plays a significant role in designing

high-speed racing and sports cars. In the current work, the same was implemented on common passenger car to attain better fuel efficiency and performance. When the vehicle is moving, there is an interaction between the air flow and the surface of the vehicle which affects fuel consumption, performance, and stability of the vehicle. Therefore, aerodynamic design judges the way in which the air flow controls cooling the engine, transmission, brake, and condenser. In the meantime improving the performance of directional and crosswind stability when the vehicle runs at high speed. It provides better comfort for the passenger such as ventilation, air conditioning, reduces dirt mud deposition on the vehicle and minimizes the wind noise. Road vehicle aerodynamics had been summarized by A R Barnard *et al.* (2014). And Hucho and Sovran (1993), who gave a comprehensive treatment. Major efforts in vehicle aerodynamic were undertaken during 1980's, research was mainly focused on drag reduction, and there was little work on aerodynamic lift. Fuel consumption is adversely affected due to aerodynamic forces (i.e., drag force). About 30 % to 50 % of fuel energy is lost due to aerodynamic force. Rakibul Hassan *et al.* (2014). emphasized various aspects of drag reduction techniques by modifying the underbody shape and redirected the exhaust gas to the rear side of the vehicle. Hence drag reduction up to 22% was achieved by underbody modification techniques, and redirection of exhaust gas reduces up to 9 % drag.

Shankar G *et al.* (2018). carried out both numerical and experimental studies on sedan car model using active airflow modification technique for reducing aerodynamic drag coefficient and lift coefficient. The analysis was performed with three delta shaped vortex generators mounted at the roof end of sedan car model where the flow separation initiates from the exterior surface of the car. The experimental results show that 4.53% and 2.55% reduction of drag coefficient and lift coefficient respectively. Inchul Kim and Hualei Chen (2010). discussed the numerical studies on reduction of aerodynamic forces on a minivan using pocket type vortex generator. The effect of vortex generator was investigated without creating the addition of drag force.

Nisugi *et al.* (2004). performed a two-dimensional calculation of flow around the vehicle model for drag reduction of the vehicle by a feedback flow control system. The optimum location of flow control nozzle was decisive for most drag forces reduction. This flow control system reduced 20% of drag force and it's suitable for all kind of bluff bodies. Y.Wang *et al.* (2014). worked in computational and experimental studies on the aerodynamics of the performance of three typical rear end body shapes such as fastback, notchback, and square back car. Aerodynamic characteristics like forces and moments are measured with yaw range from -15° to 15° for three typical rear shapes of the car using a wind tunnel. Computational and experimental investigations result reveals that the fastback has very low aerodynamic drag. It simultaneously induces positive lift which causes instability at high speed and induces bad crosswind stability.

A. Kourta *et al*. (2009) investigated the air flow separation control on the vehicle by using active fluidic control actuator to reduce consumption of fuel and emissions of gas. The results show that the aerodynamic drag coefficient of vehicles are very close to 0.20 and reduces the emission of CO_2 at least about 12 grams per kilometre by attaching fluidic control actuator.

Alamaan Altaf *et al*. (2014). discussed reduction of drag on square back road vehicles like trucks and buses. They used elliptically shaped flap with the optimal mounting angle of 50° for reducing drag force on the vehicle. Hence maximum drag reduction of 11% was achieved when they attached elliptical flaps on the vehicle. They also experimented on the vehicle with different types of flaps like triangular shape, rectangular shape flaps. Howell *et al.* (2015). investigated aerodynamic characteristics of different types of the car body, i.e., hatchback, square back and fastback car at different yaw angles using computational analysis. From the computational results both side force, lift force and stability of the vehicle had predominantly changed due to the influence of different yaw angles.

Jelf Howell *et al*. (2013). discussed the reduction of aerodynamic drag on cars using modified car shapes like a tapered rear upper body on roof and sides. Pressure distribution and flow visualization of wake studies were done using PIV. Recently, they investigated the reduction of force on a modified Ahmed body with base cavities. Barnard *et al.* (2009). did a few experiments on base flow injection which is suitable for a bluff body vehicle using a low-velocity bleed flow.

The aerodynamic drag of medium size of the car is nearly 80% of its total resistance while its moves around 100km/h. Generally the power of the vehicle directly proportional to the cubic velocity of the car. At higher speed the aerodynamic drag influences nearly 50% of fuel consumption. The relation between change in fuel consumption and change in drag coefficient is

$$\frac{\Delta FC}{FC} = \eta \times \left(\frac{\Delta C_D}{C_D} + \frac{\Delta A_f}{A_f} + 3\frac{\Delta U}{U} \right) \tag{1}$$

where FC is Fuel consumption, A_f cros section of vehiclthe e, η is the property of driving vehicle which is approximatly 0.5 to 0.7 for car driving at highway speed and U is the speed of the vehicle. In this article, the above equation was used to predict fuel consumption from drag coefficient. Experimental works are performed to analyse the aerodynamic drag force of a car and suggested the ways to reduce the aerodynamic forces by eliminating wake region on the rear side of the car using base bleed which is located at the optimum position.

2. AERODYNAMIC FORCES ACTING ON THE CAR

Vehicle aerodynamics is the study of vehicle body moving through the air and the interactions which

take place between the body surface and the air with different relative speeds. Aerodynamic forces do not affect at low speeds. However, when speed is increased, air resistance will also increase (Drag α Velocity^2). In a car body, overall aerodynamic drag consists of 75% of pressure drag. The remaining drag is due to skin friction drag and rolling resistance.

The Cartesian coordinate system with X, Y and Z axes in the car is shown in Fig. 1. When the car is moving in the forward direction, the aerodynamic forces of the car such as Lift Force (L), Drag Force (D) and Side force (S) are acting at the centre of gravity of the car along the direction of X, Y, and Z axis respectively.

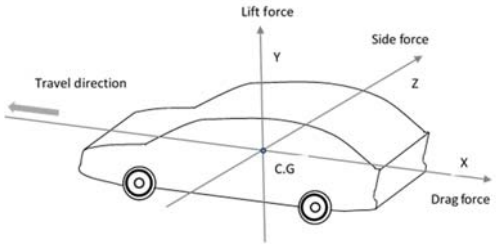

Fig. 1. Aerodynamic forces acting on the car

All the mean force coefficients are referred to the frontal area of the car and aerodynamic force coefficients are calculated using the following equation by Barnard *et al.* (2001):

$$C_D = \frac{D}{\frac{1}{2}\rho U^2 A_f} \tag{2}$$

$$C_L = \frac{L}{\frac{1}{2}\rho U^2 A_f} \tag{3}$$

$$C_S = \frac{S}{\frac{1}{2}\rho U^2 A_f} \tag{4}$$

where C_D, C_L, and C_S are coefficients of drag, lift and side force respectively; ρ is the density of air; U is air velocity (Car speed in real condition); A_f is the frontal area of the car. Aerodynamic forces i.e., Lift Force (L), Drag Force (D) and Side force (S) are measured at zero yaw angle by three component external load cell balance with an average time interval of 120 seconds.

2.1 Types of Rear End Car Body

Cars are classified according to their design, comfort, engine, capacity, aerodynamic flow, etc. Depending on the aerodynamic flow over a rear body, the cars are categorized into the hatchback, sedan, square back, and fastback as shown in Fig. 2 (Hucho and Sovran (1993)).

A car with a rear end slope angle ranging from 50^0 to 90^0 is called a square back car. This type of car's rear side has almost constant low negative pressure wake region. When rear slope angle is reduced to 22^0 or less, the body profile is known as fastback car, which has lower drag coefficient because of airflow over the roof and rear downward slope surface air stream remains attached to the body like streamline body.

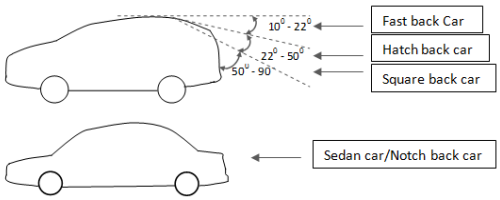

Fig. 2. Different types of rear end car body

When rear slope angle ranges from 50^0 to 22^0 then it is known as hatchback car. This type of car's rear side has more low negative pressure wake region compared to fastback and sedan car. Notchback or sedan car has a stepped rear end body. In such cars, the rear window is inclined downward to meet horizontal rearward extending boot.

Among all the types of rear end car body, hatchback model was preferred by most of the people due to its lower cost. While moving, airflow on the hatchback car creates more wake region which arises a large amount of drag at its rear end when compared to other models (Heinz Heisler (2002)). Hence hatchback car model was preferred in our work and the proposed method to reduce drag was effective in this model which in turn reduces the fuel consumption effectively.

3. EXPERIMENTAL SETUP

1:12 scaled car models are realized based on the blockage ratio that should not exceed the limit of 7.5% (Katz *et al.* (2006)). The blockage ratio of a wind tunnel for this model is 4.75 %. Therefore, the effect due to blockage ratio is negligible.

The scaled models are tested in the wind tunnel laboratory at Madras Institute of Technology. The wind tunnel has a test section 4 ft wide x 3 ft high x 5 ft long. The maximum velocity is 40 m/s approximately and the contraction ratio is 9:1. Air velocity U is measured with the pitot-static tube, which is attached to the ceiling of the wind tunnel test section (Hwang *et al.* (2016)). The aerodynamic forces acting on the scaled models are measured with external balance for various speeds. The car model is fixed to three component balance through the platform acting as a road at connecting points under the rear and front wheels, as shown in Fig. 3. The platform is built to simulate the road condition at such height so has to provide more uniform flow from the bottom of wind tunnel test section and also ensure that the model is outside the boundary layer (0.99U). The leading edge of the platform is sharpened to create a smooth start of the boundary layer, as shown in Fig. 3a. (Zhang *et al.* (2012)). The hatchback type of car model used in the wind tunnel test is shown in the Fig. 3b. The model is 23 cm long, 15 cm wide, 10 cm high and overall dimensions represent the scale down (1:12) of a real hatchback car.

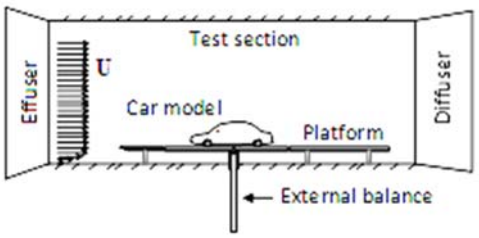

Fig. 3a. Experimental setup with car model

Fig. 3b. Car model mounted in the wind tunnel

3.1 Base Bleed Attachment

Generally, the drag force on car occurs due to car profile design and its surface. When air flows on the surface, flow separation takes place and it will induce major pressure on the rear side. Therefore, this will produce large wake on the rear side of the car increasing the overall drag. The flow separation happens due to lack of energetic flow and inability of flow to move past the sharp corner. In the car body, profile drag (wake and skin friction) contributes 80–90% of total drag hence, it is more important to eliminate the wake region at the rear side of the car. Therefore, attaching the basebleed eliminates the wake region at the rear side of the car.

The basebleed consists of two converging hollow tubes and the cross-section area of front side tube is greater than the rear side. Both tubes inject low-velocity air at the rear side by sucking the air from the front side. These hollow tubes are located under the floor of the car as shown in Fig. 4 without disturbing any existing system or structure of the car. An experimental test is conducted to optimize the following parameters with basebleed.

1. Distance between two converging hollow tubes at the front side (B_f).
2. Distance between basebleed tubes at the rear side (B_r).
3. Distance between ground (Road surface) and basebleed at the front side (H_f).
4. Distance between ground (Road surface) and basebleed at the rear side (H_r).

3.2 Measurement of Pressure Distribution

The pressure distribution along the surface of the car model was measured with and without basebleed. Forty pressure taps (P1 to P40) was impinged on the exterior surface of the car model along the centre line and connected with digital scanning array (DSA) for precise measurement. The schematic sketch of the model of the car with ports was shown in Fig. 5.

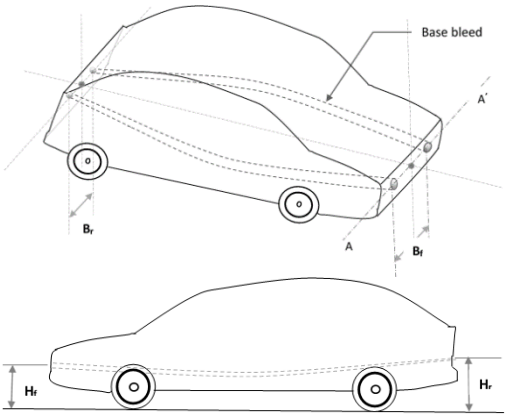

Fig. 4. Attachment of Base bleed in the car model.

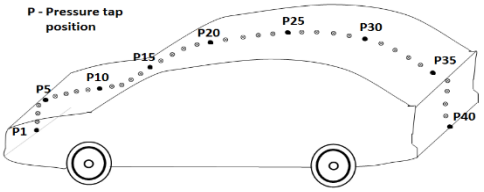

Fig. 5. Schematic sketch of the car model with pressure taps

4. RESULT AND DISCUSSION

Generally, when a car moves forward at speed above 60 Kmph, high-pressure and low-pressure zones are created at the front and rear side of the car respectively. If the velocity of the car increases, the stagnation pressure also increases and at the same time rear side pressure decreases. This low-pressure region is created due to flow separation and generation of vortices at the rear side (Lamond *et al*. (2009)). Due to the implementation of basebleed in the car, the flow separation will be delayed on the car surface and also wake is removed entirely due to the creation of pressure energy in the form of fluctuation energy. Fluctuation energy is created by the entry of air through both the basebleed tubes which hits the wake region directly. The drag force is reduced by air sucked from the front side of the vehicle. This, in turn, will create low-pressure zone at the front side of the car. The air can flow from the basebleed at different speeds and the flow is directed towards low-pressure zone so that it can reduce the negative pressure and increase the reduction of drag. The basic model is tested at free stream velocity of 20 m/s and C_D value is found to be 0.3329. Figure 6 shows the comparison of pressure coefficient of base car configuration with the implementation of base bleed in the car and reference curve from Hucho and Sovran (1993).

The effect of the pressure distribution of car model is shown in Fig. 6. From this graph, it can be seen that the coefficient of pressure curve of the car with base bleed configuration is lower than Cp curve of base car configuration between port number 1 to 12 (Front side region). This is due to air sucked from the front side of the vehicle. Between port number 22 to 40 (Rear side region) Cp curve of the car with basebleed configuration lies above Cp curve of base

car configuration. Thus basebleed exhaust air is filling up low-pressure zone at the rear side of the car. This pressure distribution curve shows the function of basebleed by increasing the pressure on the rear side region of the car and decreasing of the pressure at the front side region. As a result overall drag is reduced. The pressure on the backside, as well as the front side of the car, are changed considerably due to basebleed attachment. Therefore conclude that if the implementation of basebleed in car predominantly reduce the aerodynamic drag and as well as improve the stability of the car.

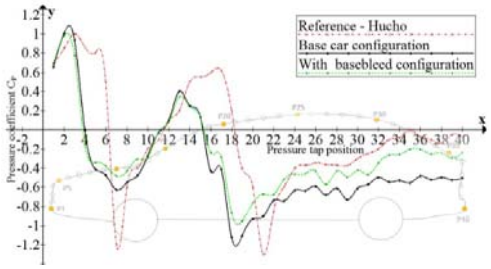

Fig. 6. Comparison of pressure coefficient curve of the car.

Table 1 Value of Aerodynamic coefficient

	Aerodynamics Coefficients		
	C_D	C_L	C_S
Base Car configuration	0.3329	0.1492	0.106
With Base bleed configuration	0.3123	0.1491	0.106

With the attachment of base bleed car model tested at free stream velocity of 20 m/s, C_D value is reduced to 0.3123 from 0.3329, but the coefficient of lift and side force does not change significantly. The basebleed location has been optimized by conducting the wind tunnel tests with different positions of basebleed by varying the distance between two base bleed tubes from (B_f) 500 mm to 1700 mm at the front side and 350 mm to 1000 mm on the rear side of the car (B_r). The distance between ground (Road surface) and Basebleed at the front side are varied from (H_f) 350 mm to 750 mm and at the rear side of the car from (H_r) 350 mm to 750 mm.

Initially, the distance between the base bleed was maintained at 500mm and then gradually increased up to 1400mm at the front side. In the meantime, the distance between the base bleed at rear side was maintained constant at 750mm for all the cases. The pressure distribution along the surface of the car was noted which was shown in Fig. 7 (a). The overall drag reduction of the car depends on the pressure distribution mainly at its front and rear side. At the front side (port P1 – P7), the pressure was found the minimum, if the distance between the base bleed (B_f) was maintained constant at 1200mm when compare to other cases. The position of the basebleed at B_f = 1200mm is near to the blended corner of the car, at that point air will be sucked more effectively when compared to other cases. In turn reduction in pressure, coefficient was noted and the airflow was streamlined. The above statement was supported by the pressure distribution observed at the rear side (port P25 - P40) where the pressure is maximum. To countercheck, the result obtained, the separate experiment was conducted with the help of three component balance. The result obtained was shown in Fig. 7 (b), the same B_f = 1200mm shows minimum drag coefficient 0.3142 which concretes the result obtained in Fig. 7 (a).

In the Figs. 7 (a) and 7 (b) the optimized position for locating basebleed along the x-axis at the front side of the car was found. At the rear side, the same experiment was repeated with basebleed location fixed at the front side (B_f = 1200mm) and the optimized location was found at B_r = 350mm along X-axis and its corresponding drag coefficient was 0.3124. But the variation in basebleed location at the rear side was not affected by the pressure distribution at the front side which was shown in Figs. 8 (a) and 8 (b). The next set of experiments was repeated to finding out the suitable location for basebleed from the ground (along Y-axis) for both front and rear side of the car by fixing the B_f and B_r values constant at 1200mm and 350mm. H_f = 450mm at the front side and H_r = 550mm at the rear side shows the better result when compared to other locations which were shown in Figs. 9 (a)&(b) and Figs. 10 (a)&(b). The height variation of basebleed location was not affected by the drag coefficient (0.3123) of the car which was in minimum level.

The optimum position for installing basebleed in the car was found at both the front and rear side of the car. At this proposed location of basebleed, the flow

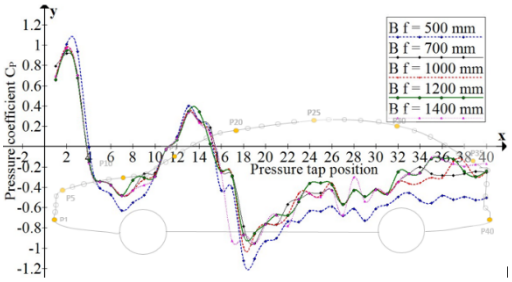

(a) Pressure tap position Vs Pressure Coefficient

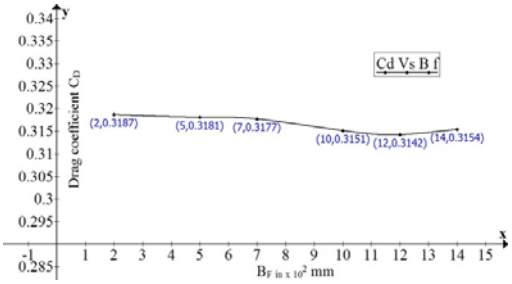

(b) B_F Vs Drag Coefficient

Fig. 7. (a) Variation of pressure coefficient with respect to the distance between two hollow tubes (basebleed) at front side & 7 (b) Variation of drag coefficient with respect to the distance between two hollow tubes (basebleed) at the front side

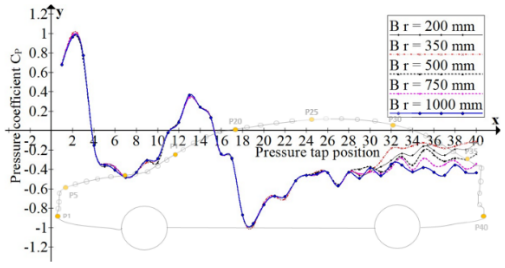

(a) Pressure tap position Vs Pressure Coefficient

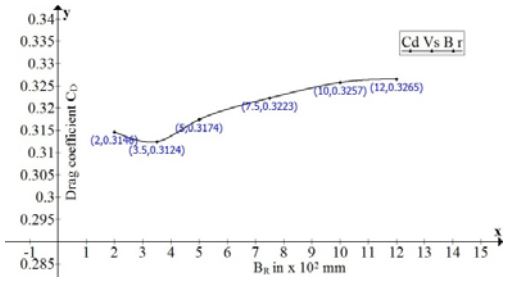

(b) B_R Vs Drag Coefficient

Fig. 8. (a) Variation of pressure coefficient with respect to the distance between two hollow tubes (basebleed) at rear side & 8 (b) Variation of drag coefficient with respect to the distance between two hollow tubes (basebleed) at the rear side

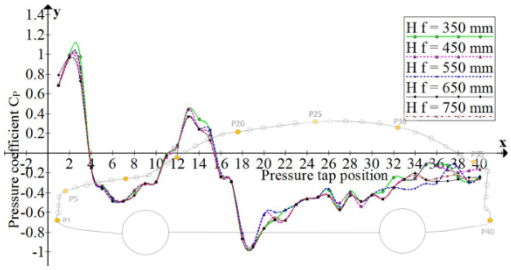

(a) Pressure tap position Vs Pressure Coefficient

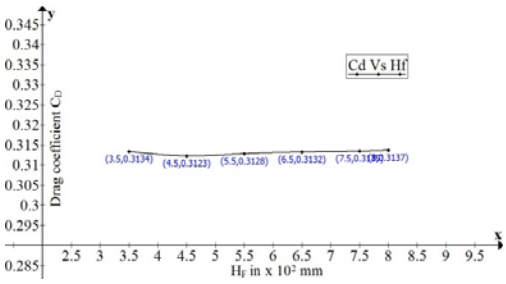

(b) H_F Vs Drag Coefficient.

Fig. 9. (a) Variation of pressure coefficient with respect to the distance between ground (road surface) and basebleed at front side & 9 (b) Variation of drag coefficient with respect to the distance between ground (road surface) and basebleed at the front side

separation on the surface of the car will not occur immediately due to the suction of air at the front side. Fluctuation energy was created at the rear side of the car due to blowing of air at the rear side which removes the wake region entirely. Due to the absence of wake region, the streamline flow was created around the car which helps to improve its stability and performance. In the meantime, the suction of air at the front side creates low-pressure zone which also supports to reduce the overall drag force acting on the car.

The maximum rate of reduction in drag coefficient achieved was 6.188% by installing basebleed at the proposed location in the car model. In turn, fuel consumption was reduced up to 4.33% in the real hatchback car running at 70 km/h.

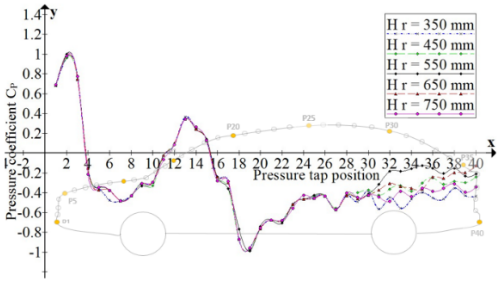

(a) Pressure tap position Vs Pressure Coefficient

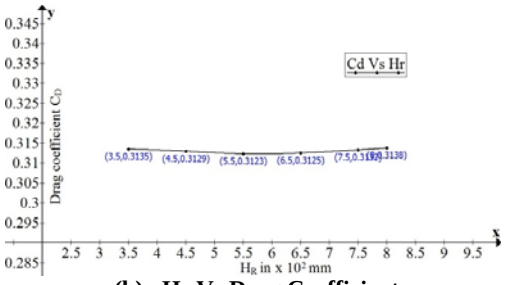

(b) H_R Vs Drag Coefficient

Fig. 10. (a) Variation of pressure coefficient with respect to the distance between ground (road surface) and basebleed at rear side & 10 (b) Variation of drag coefficient with respect to the distance between ground (road surface) and basebleed at the rear side

5. CONCLUSION

This article discusses the aerodynamic coefficient of car model with the attachment of basebleed at optimized locations by wind tunnel testing. The tests were conducted for understanding the effect of flow condition on aerodynamic forces on the car to compare between the base car configuration and attachment of basebleed. From this work, the general conclusion is drawn as follows: the pressure difference between the rear and front side of the car is responsible for the major portion of aerodynamic drag of car. The aerodynamic drag coefficient of car model with the attachment of basebleed is reduced from 0.3329 to 0.3123 due to the elimination of the wake region at the rear side of the car. This basebleed also maintains the streamline, controls the lift force and air flow towards the lower pressure zone at the rear side of the car. The reduction of aerodynamic drag coefficient in hatchback cars was calculated by experiment with 1:12 scale down model. The maximum reduction of the rate in drag coefficient relative to the car without basebleed is 6.188 % for the optimized

position of basebleed given by B_F = 1200 mm, B_R = 350 mm, H_F = 450 mm and H_R=550 mm.

ACKNOWLEDGEMENTS

The authors would like to thank the Department of Aerospace Engineering at Anna University MIT Campus for their support during the wind tunnel testing and also thank the Department of Aeronautical engineering at Bannari Amman Institute of Technology for their wind tunnel testing guidance and expertise.

REFERENCES

Altaf A., A. Ashraf., Omar, and W. Asrar (2014). Passive Drag Reduction of Square Back Road Vehicles. *Journal of Wind Engineering and Industrial Aerodynamics* 134, 30-43.

Barnard, A. R., Wang, Z, Y. M. Chung (2014). Drag-Reduction Devices to Improve the Aerodynamic Efficiency of Close-Coupled Large Goods Vehicles. *Proceeding of International Vehicle Aerodynamics Conference*, *Holywell Park, Loughborough.*

Barnard, R. H., C. A. Gilkseon, H. M. Thompson and M. C. T. Wilson (2009). An Experimental and Computational Study of the Aerodynamic and Passive Ventilation Characteristics of Small Livestock Trailers. *International Journal of Wind Engineering and Industrial Aerodynamics* 97, 9–10.

Barnard, R. H. (2001). *Road Vehicle Aerodynamic Design: An Introduction*. Mechaero, United Kingdom.

Heinz, H. (2002). *Avanced Vehicle Technology*, Butterworth-Heinemann, Woburn, MA.

Howell, J. (2015). Aerodynamic Drag of Passenger Cars at Yaw, *SAE International Journal of Passenger. Cars – Mechanical System* 8(1), 1-11

Howell, J., M. Passmore, and S. Tuplin (2013). Aerodynamic Drag Reduction on a Simple Car-Like Shape with Rear Upper Body Taper. *SAE International Journal of Passenger Cars - Mechanical Systems* 6 (1), 1-9.

Hucho, W. and G. Sovran (1993). Aerodynamics of Road Vehicles. *Annual Review of Fluid Mechanics,* 25(1), 485-537.

Hwang, B. G., S. Lee, E. J. Lee, J. J. Kim, M. Kim, D. You, and S. Joon Lee (2016). Reduction of Drag in Heavy Vehicles with Two Different Types of Advanced Side Skirts. *Journal of Wind Engineering and Industrial Aerodynamics* 155, 36–46.

Inchul K. and H. Chen (2010). Reduction of Aerodynamic Forces on a Minivan by a Pair of Vortex Generators of a Pocket Type. *International Journal of Vehicle Design* 53 (4), 300–316.

Katz, J. (2006). Aerodynamics of Race Cars. *Annual Review of Fluid Mechanics* 38 (1), 27–63.

Kourta, A. and P. Gilliéron (2009). Impact of the Automotive Aerodynamic Control on the Economic Issues. *Journal of Applied Fluid Mechanics* 2(2), 69-75.

Lamond, A., J. J. Kenned, and M. T. Stickland (2009). An Investigation into Unsteady Base Bleed for Drag Reduction in Bluff Two-Box SUVs. An *European Automotive Simulation Conference, EASC, Department of Mechanical Engineering, University of Strathclyde* 6–7, UK.

Nisugi, K., T. Hayase, and A. Shirai (2004). Fundamental Study of Aerodynamic Drag Reduction for Vehicle with Feedback Flow Control. *JSME International Journal Series B* 47(3), 584–592.

Rakibul, H., S. M. Toukir Islam, A. Mohammad, and Md Q. Islam (2014). Numerical Study on Aerodynamic Drag Reduction of Racing Cars. *10th International Conference on Mechanical Engineering, ICME 2013, Department of Mechanical Engineering, Bangladesh University of Engineering and Technology, Dhaka,* 308-313.

Shankar, G., G. Devaradjane (2018). Experimental and Computational Analysis on Aerodynamic Behavior of a Car Model with Vortex Generators at Different Yaw Angles. *Journal of Applied Fluid Mechanics* 11(1), 285-295.

Wang, Y, Y. Xin, Z. Gu, S. Wang, Y. Deng and X. Yang (2014). Numerical and Experimental Investigations on the Aerodynamic Characteristic of Three Typical Passenger Vehicles. *Journal of Applied Fluid Mechanics* 7(4), 659-671.

Zhang, Y. C., J. Zhao, J. Li, and Z. Zhang (2012). Wind Tunnel Tests and Aerodynamic Numerical Simulations of Car Opening Windows. *International Journal of Vehicle Design* 58 (1), 62-73.